

*Citation for published version:*

Ginzinger, L., Sahinkaya, MN, Schindler, T, Ulbrich, H & Keogh, P 2014, 'Model-based condition monitoring of an auxiliary bearing following contact events', Paper presented at 10th International Conference on Motion and Vibration Control, MOVIC 2010, Tokyo, UK United Kingdom, 17/08/10 - 20/08/10.

*Publication date:*  
2014

*Document Version*  
Early version, also known as pre-print

[Link to publication](#)

**University of Bath**

**Alternative formats**

If you require this document in an alternative format, please contact:  
[openaccess@bath.ac.uk](mailto:openaccess@bath.ac.uk)

**General rights**

Copyright and moral rights for the publications made accessible in the public portal are retained by the authors and/or other copyright owners and it is a condition of accessing publications that users recognise and abide by the legal requirements associated with these rights.

**Take down policy**

If you believe that this document breaches copyright please contact us providing details, and we will remove access to the work immediately and investigate your claim.

4A16

## Model-Based Condition Monitoring of an Auxiliary Bearing following Contact Events\*

L. GINZINGER\*\*, M. N. SAHINKAYA\*\*, T. SCHINDLER\*\*\*, H. ULBRICH\*\*\* and P. KEOGH\*\*

\*\* Department of Mechanical Engineering, Faculty of Engineering and Design, University of Bath  
Claverton Down, Bath, BA2 7AY, United Kingdom

E-mail: ginzinger@gmail.com, m.n.sahinkaya@bath.ac.uk, p.s.keogh@bath.ac.uk

\*\*\* Institute of Applied Mechanics, Technische Universität München  
Boltzmannstr. 15, 85748 Garching, Germany

E-mail: schindler@amm.mw.tum.de, ulbrich@amm.mw.tum.de

### Abstract

Auxiliary bearings are used in many rotor systems, e.g. those with active magnetic bearings. In a case of a contact with the auxiliary bearing, high impact forces and wear are possible. Therefore the auxiliary bearings have to be replaced after a certain number of contact events. This is very costly and often needs complete dismantling of the rotor system.

In this paper a concept for model based condition monitoring of an auxiliary bearing is developed. The rotor system is modeled in a multibody simulation environment, including the contact to the auxiliary bearing and various fault parameters. After contact (drop or bouncing contact) occurs in the real rotor system, an identification algorithm analyses the measuremental data of the contact event and determines the fault which occurred. Based on the results of the identification algorithm, an optimization tool aligns the rotor simulation with the measurement by varying the fault parameters. After the alignment of the simulation, the simulation results are evaluated. The contact forces are evaluated against location on the surface of the auxiliary bearing and are stored. This procedure is performed after each contact event. Hence, a weighting of the load over the surface of the auxiliary bearing is gained. Depending on the material and structure, these data can be used for a life-time estimation of the auxiliary bearing. Using an active magnetic bearing test facility, the monitoring system has been successfully tested.

**Key words** : model-based monitoring, auxiliary bearings, condition monitoring, contact, non-smooth mechanics, multibody simulation, unilateral contact.

### 1. Introduction

Active magnetic bearings (AMBs) provide efficient and contact free levitation of rotors and have many advantages compared with oil film bearings. However, due to their limited force capacity, they have to incorporate auxiliary bearings to protect the rotor and stator laminations in the case of large rotor vibrations. Depending on the impact condition, auxiliary bearings may sustain high impact forces during contact resulting contact stresses, temperatures and strains. Therefore they have to be replaced after a certain number of contact events. Also contact events necessitate machine shut-downs. Replacement of auxiliary bearings requires the machine to be taken out of service and dismantled. This is costly and therefore there is a need to assess the condition of the auxiliary bearings after each contact without dismantling the machine. Improvements in the reliability of magnetic bearings are of current research interest and are essential to extend the application areas of these bearings to safety critical systems in aerospace, automotive and manufacturing industries. Magnetic bearings usually incorporate a processor for control purposes, and can be used as bearings, actuators

and sensors. Therefore, they form an essential part of a system monitoring and fault detection system<sup>(15)</sup>. Many research activities have concentrated on developing adaptive magnetic bearing controllers to prevent the rotor contact with auxiliary bearings under transient loading, or if the contact does occur, to minimize the impact damage and to recover the rotor position as quickly as possible without the necessity to shut down the system<sup>(19),(20)</sup>. Fault detection and tolerance systems mainly concentrate on identifying faults in sensors or magnetic bearing coils, and are usually based on a stochastic approach<sup>(16),(17),(18)</sup>. SAHINKAYA,<sup>(11)</sup> investigated fault detection at rotor systems with active magnetic bearings. Using stochastic methods, various faults like transducer malfunctions, signal-processing failures or unbalances are identified. HECKMANN,<sup>(12)</sup> published a work regarding the identification of unbalance and misalignment. Only the signal of the rotor orbit is used for this identification. However, there is no work reported on identifying the condition of the auxiliary bearings, which are inactive during the normal operation of the magnetic bearings, and hence their condition cannot be detected by the existing sensors in the system. Therefore, a model based condition monitoring system is proposed here to identify the condition of the auxiliary bearings after each impact, and detect when they are required to be replaced.

## 2. Concept of the Condition Monitoring

The concept for model-based condition monitoring of auxiliary bearings is based on the concept of HECKMANN,<sup>(12)</sup>.

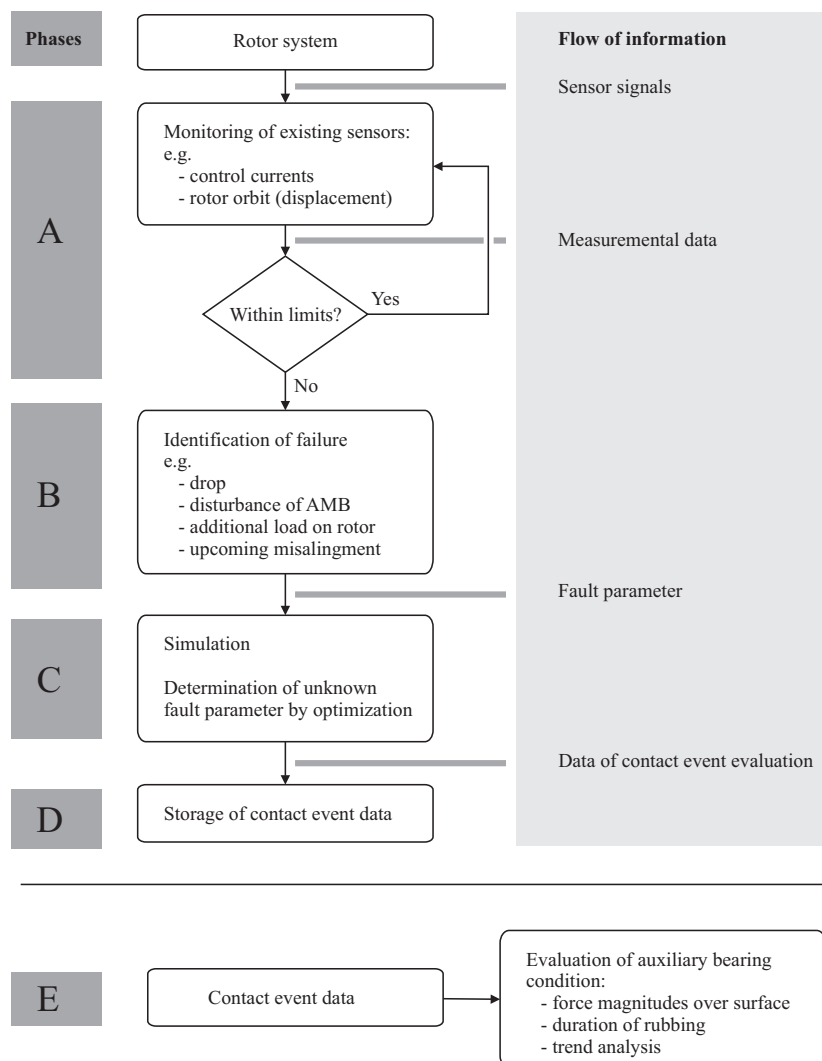


Fig. 1 Concept for a model-based condition monitoring system

The scheme, shown in Fig. 1, consists of various phases, which are labeled by A to E.

### 2.1. Phase A: Monitoring

During normal operation of the rotor system, a monitoring system, which already exists in many cases, observes the signal of existing sensors e.g. control currents of active magnetic bearings and the rotor orbit. As long as the measured signals are within the tolerable range of operation, Phases B to E are on stand-by. When the limits following a contact event are exceeded, the floating measurement of the observed signals is captured and transferred to Phase B. It is essential that the floating measurement comprises the data starting at the beginning of the disturbance.

### 2.2. Phase B: Identification of failure

In a first step, the measured signals of the contact event are evaluated using case differentiation and statistical models. There has been some previous work on identifying various failures at rotor systems<sup>(11), (12)</sup>.

For the present paper, some defects are embedded in the identification algorithm in Phase B, which reduces possible faults down to the fault which led to rubbing. Depending on the application and the faults, various defect characteristics, which are used for the identification, are distinguishable. These can be based on stochastic values, mean values and others in time as well as in the frequency domain. The defect characteristics are calculated from the measured signals. In the following the list of embedded faults, and defect characteristics (in brackets) is given.

#### Fault at the active magnetic bearing (AMB)

- Cut-off of channel(s) of AMB: *(All control currents are evaluated piecewise. If one becomes zero, a cut-off of the corresponding channel is detected.)*
- Disturbance of the control currents: *(If there is a significant change in the signal of the control currents just before there is a change in the signal of the rotor deflection, a disturbance of the amplifier of the AMB is detected. The additional arising frequency is one of the fault parameters.)*

#### Fault at the rotor

- Changing unbalance: *(The mean radius of the rotor orbit increases/decreases.)*
- Misalignment between rotor and drive system: *(The center of the mean radius moves, while the average of the radius amplitude does not increase. The angle of the movement of the center is one of the fault parameters.)*

The selection of suitable defect characteristics also depends on the available sensor information. In the presented example, the following signals are used to determine the type of fault:

- Rotor orbit (i.e. rotor deflections) at an AMB
- Control currents of an AMB

The identification of the fault determines the fault parameters, depending on the defect, e.g. in the case of a cut-off of one or more of the AMB channels, the fault parameter is known. It is a function of the control current, which is zero. Unknown fault parameters are determined by the optimization algorithm in Phase C.

The procedure of the identification algorithm in this case is shown in Fig. 2.

The output of the identification process, the type of fault, the fault parameter (known and unknown) as well as the measurement is transferred to Phase C. If no embedded fault can be determined, the concept exits at this point due to a non-modeled fault.

### 2.3. Phase C: Simulation, Optimization

The simulation environment used in this phase, has to be successfully aligned with the

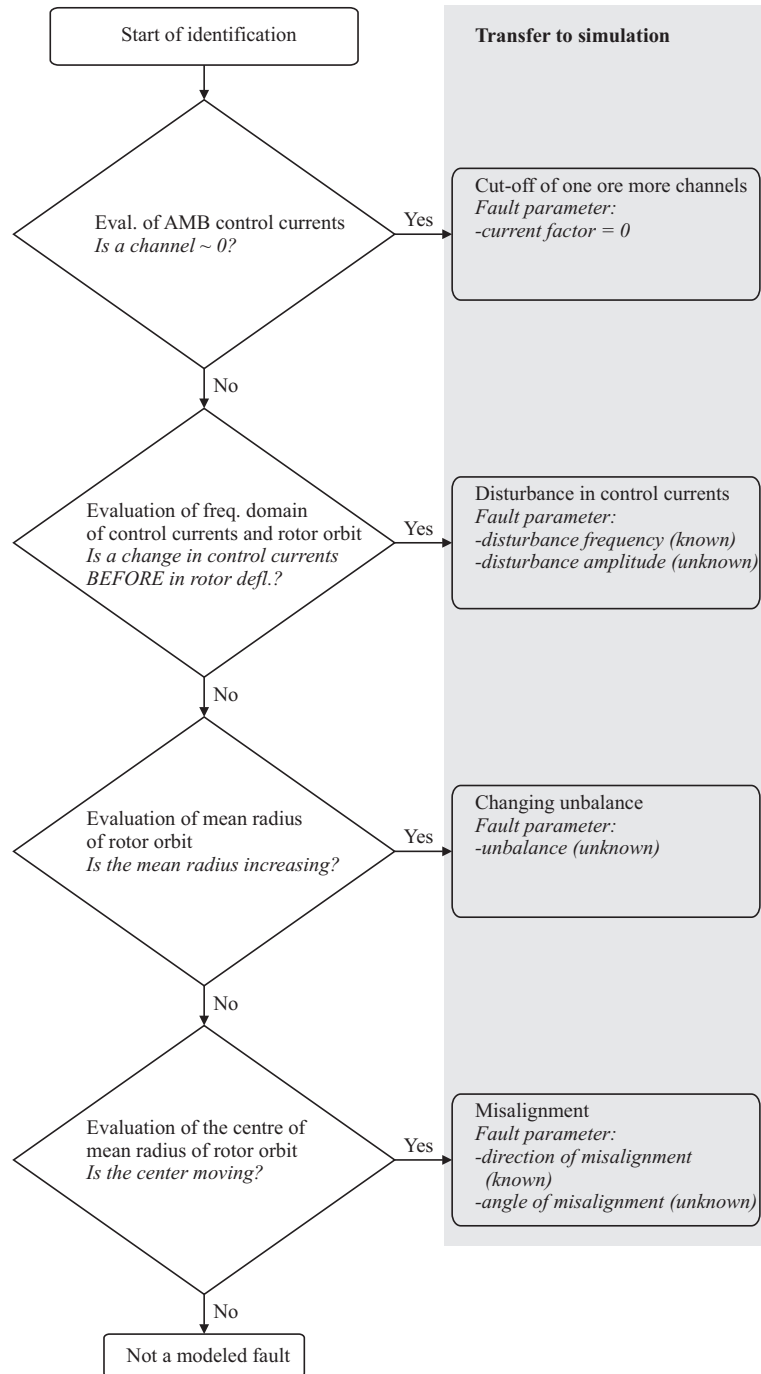


Fig. 2 Procedure of identification of a fault (Phase B)

initial undamaged rotor system. All defects, which should be included in the concept, have to be included in the modeling. If the condition of the system changes over the lifetime, some of the parameters of the simulation have to be regarded as time-variant, e.g. the friction in the auxiliary bearing.

Using the data from the identification process, all parameters of excluded faults are set to the initial (undamaged) value. All known fault parameters are set in the simulation model. Solving for the unknown fault parameters and the time-variant and therefore unknown parameters of the model determines the optimization problem. In the present case, the time-variant parameter is the friction of the contact. The cost function, which is used to compare simulation and experiments for the optimization, has to represent the contact event. The most important characteristic of the contact event is the dominant rubbing state. Three cases will

be distinguished:

- (1) Swinging on the bottom of the auxiliary bearing (swinging)
- (2) Swinging + Temporarily full annular rub in forward direction (forward rub)
- (3) Sw. + Fw. rub + Temporarily full annular rub in backward direction (backward rub)

The dominant state is in the first case (swinging). In the second case, it is rubbing in the forward direction and in the third case it is rubbing in the backward direction. There will always be temporarily forward rubbing before the transition to backward rubbing, but not vice versa. Hence, there is an increasing dominance of the rubbing states, swinging  $\rightarrow$  forward rub  $\rightarrow$  backward rub, which also represents increasing damage to the system. For a detailed discussion of the various rubbing states, refer to<sup>(14)</sup>.

The cost function should reflect the occurrence of these three cases. For this reason, an evaluation of contact locations in polar coordinates is proposed (the origin of the coordinate system is the center of the undeformed rotor shaft). The slope of the polar angle clearly shows the occurrence of the particular rubbing state. In case of an oscillation around zero the state is swinging, in case of a positive value, it is forward rubbing and backward rubbing is indicated by a negative slope. The slope should be determined from the filtered polar angle.

The duration of the occurrence of the certain rubbing states are evaluated from the slope. The duration of the swinging state is calculated from the time, where the slope is in the vicinity of zero. The duration of the state forward rub is taken from the duration of a positive slope and the duration of the state backward rub from a negative slope. The proposed cost function is calculated as follows:

$$f_{cost} = c_{swing}t_{swing} + c_{fwrub}t_{fwrub} + c_{bwrub}t_{bwrub} \quad (1)$$

where  $c_{swing}$ ,  $c_{fwrub}$  and  $c_{bwrub}$  are the coefficients of the swinging state, the forward rub state and the backward rub state, respectively.  $t_{swing}$ ,  $t_{fwrub}$  and  $t_{bwrub}$  are the respective durations of the states. To take the increasing dominance of certain states (as described) into account, the coefficients are chosen in the following ascending order:

$$c_{swing} \ll c_{fwrub} \ll c_{bwrub} \quad (2)$$

The comparison of the contact event in the measurement and the simulation can be performed using this cost function.

In this approach, the optimization algorithm uses the implicit filtering method. Implicit filtering is a projected quasi-Newton method for bound constrained optimization problems. The gradients are computed with a finite difference and the difference gradient varies as the optimization progresses. A detailed discussion is given by KELLEY<sup>(13)</sup>.

#### 2.4. Phase D: Storage of a contact event

After the optimization finishes, the simulation data of the contact event are stored. These data comprise:

- Contact forces vs. time,
- Rotor orbit vs. time,
- Orbit of auxiliary bearing vs. time,
- Rotor speed.

#### 2.5. Phase E: Evaluation of auxiliary bearing condition

In the second part of the concept, the actual condition of the auxiliary bearing is evaluated after each contact event. The analysis of the contact forces and the orbits can vary depending on the application and the type of auxiliary bearings. In this paper the sum of forces vs. polar angle of the contact point is evaluated.

For a certain application of an auxiliary bearing, further investigations have to be performed, to estimate the life-expectancy, e.g. a correlation between the sum of forces vs. polar angle of the contact point and the wear inside the auxiliary bearing.

### 3. Simulation Environment

The simulation environment MBSim (<http://mbsim.berlios.de>), which was developed at the Institute of Applied Mechanics, is used for the concept. This simulation library is licensed under *GNU Lesser General Public License (LGPL)*. MBSim is based on a framework for the efficient simulation of multibody systems with unilateral contacts and elastic elements. The framework comprises the description of the system dynamics as well as numerical methods as provided in<sup>(3),(5)</sup>. A brief overview is now given. For a more comprehensive introduction to the formulation and numerics of non-smooth dynamics see<sup>(1),(4)</sup>.

#### 3.1. Non-smooth Dynamics

The non-smooth dynamics of the system are described in terms of a measure differential equation. The dynamics of a bi- and unilateral constrained system can be expressed by

$$\mathbf{M}d\mathbf{u} = \mathbf{h}dt + \mathbf{W}d\Lambda. \quad (3)$$

The matrix  $\mathbf{M} = \mathbf{M}(\mathbf{q})$  denotes a symmetric, positive definite mass matrix and depends on the  $f$ -dimensional vector of generalized coordinates  $\mathbf{q} \in \mathbb{R}^f$ . The vector  $\mathbf{u} = \dot{\mathbf{q}}$  denotes the velocity vector. The acceleration measure

$$d\mathbf{u} = \dot{\mathbf{u}}dt + (\mathbf{u}^+ - \mathbf{u}^-)d\eta \quad (4)$$

is the sum of the continuous part  $\dot{\mathbf{u}}dt$  and the discrete parts  $(\mathbf{u}^+ - \mathbf{u}^-)d\eta$ . The second term is the difference of the left and the right limit of the velocities weighted by the sum of the DIRAC delta functions  $d\delta_i$  at the discontinuities  $t_i$ :

$$d\eta = \sum_i d\delta_i, \quad (5)$$

$$d\delta_i = d\delta(t - t_i) = \begin{cases} \infty & \text{if } t = t_i \\ 0 & \text{if } t \neq t_i \end{cases}. \quad (6)$$

On the right hand side of equation (3) the vector  $\mathbf{h} = \mathbf{h}(\mathbf{u}, \mathbf{q}, t)$  contains all smooth external, internal and gyroscopic forces. The reaction measure in the contacts  $\mathbf{W}d\Lambda$  is decomposed by the generalized force directions  $\mathbf{W} = \mathbf{W}(\mathbf{q})$  and the magnitudes  $d\Lambda$ . In analogy to the acceleration measure, the reaction measure  $d\Lambda$  contains forces  $\lambda$  due to persisting contacts as well as impulses  $\Lambda$  due to collisions of bodies at the impact times  $t_i$ :

$$d\Lambda = \lambda dt + \Lambda d\eta. \quad (7)$$

Integrating (3) under consideration of the DIRAC delta (5) yields the classical equations of motion for a constrained system and the impact equations.

The computation of the accelerations  $\dot{\mathbf{u}}$  as well as the post-impact velocities  $\mathbf{u}_i^+$  in equation (3) requires knowledge of the unknown contact reactions  $\lambda$  and  $\Lambda_i$ , respectively. Thus, additional contact laws must be constituted. Contacts between bodies in the system are modeled as discrete point contacts whereby the contact zone is assumed to be totally rigid. Deformations of elastic components are only regarded in form of the overall discretization, no local deformation e.g. of a beam cross-section is modeled. Consequently, a contact corresponds to a constraint. In this context two different types of contacts are considered, for which different contact laws hold: persisting contacts which are always closed; and contact that may be open or closed.

The contact reactions

$$\mathbf{W}d\Lambda = (\mathbf{W}_N \quad \mathbf{W}_T) \begin{pmatrix} d\Lambda_N \\ d\Lambda_T \end{pmatrix} = (\mathbf{W}_B \quad \mathbf{W}_U \quad \mathbf{W}_T) \begin{pmatrix} d\Lambda_B \\ d\Lambda_U \\ d\Lambda_T \end{pmatrix} \quad (8)$$

are decomposed into components normal (index N) - split up in bilateral (B) and unilateral (U) - and tangential (T) to the contact plane.

### 3.2. Dynamics between Impacts

First of all, only smooth motion is considered, i.e. no impacts occur. Then a bilateral contact implies a bilateral constraint of the form

$$g_B = 0, \lambda_B \in \mathbb{R}, \quad (9)$$

where  $g_B$  denotes the normal distance of the interacting bodies in the contact point. The second type of contact also allows for detachment. The associated unilateral constraint is given by the SIGNORINI-FICHERA-condition

$$g_U \geq 0, \lambda_U \geq 0, g_U \lambda_U = 0. \quad (10)$$

The respective force laws are shown in Figs. 3 a and 3b.

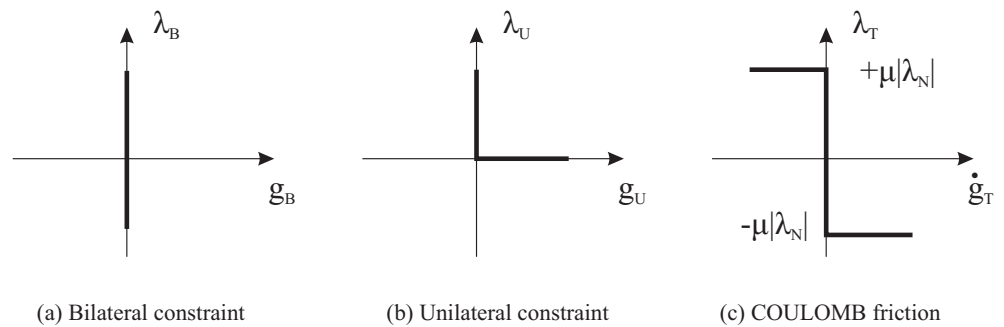


Fig. 3 Force laws for bi- and unilateral contacts and friction

For both bi- and unilateral constraints, dry friction is considered. In order to establish COULOMB'S law, the force of a single contact is decomposed in a component  $\lambda_N \in \{\lambda_B, \lambda_U\}$  normal to the contact plane and – in case of three dimensional dynamics – tangential components  $\lambda_T$  in friction direction. Using the relative tangential velocity  $\dot{g}_T$ , COULOMB'S friction law is given by

$$\text{if } \dot{g}_T = 0 \Rightarrow |\lambda_T| \leq \mu_0 |\lambda_N| \quad (11)$$

$$\text{if } \dot{g}_T \neq 0 \Rightarrow \lambda_T = -\frac{\dot{g}_T}{|\dot{g}_T|} \mu |\lambda_N|. \quad (12)$$

For the planar case, the force law of a tangential frictional contact is plotted in Fig. 3c.

### 3.3. Impact dynamics

In contrast to persisting and detaching contacts, a closing contact implies a discontinuity in the relative and therewith possibly all generalized velocities. Therefore impacts must be treated separately. The effect of an impact of a specific contact may concern all other constraints, the bilateral as well as the unilateral types.

The impact law for a bilateral contact is given by

$$\dot{g}_B^+ = 0, \Lambda_B \in \mathbb{R} \quad (13)$$

and ensures that relation (9) is not violated after collisions. Given on impulsive level, NEWTON'S impact law in the formulation of MOREAU:

$$\dot{g}_U^+ \geq 0, \Lambda_U \geq 0, \dot{g}_U^+ \Lambda_U = 0 \quad (14)$$

and COULOMB'S friction law with the normal reaction  $\Lambda_N \in \{\Lambda_B, \Lambda_U\}$ :

$$\text{if } \dot{g}_T^+ = 0 \Rightarrow |\Lambda_T| \leq \mu_0 |\Lambda_N| \quad (15)$$

$$\text{if } \dot{g}_T^+ \neq 0 \Rightarrow \Lambda_T = -\frac{\dot{g}_T^+}{|\dot{g}_T^+|} \mu |\Lambda_N| \quad (16)$$

hold for active contacts (i.e.  $g_N = 0$ ) only.

### 3.4. Elastic components

There are many modeling possibilities for elastic beams available in the literature<sup>(6)</sup>. A co-rotational model<sup>(7)</sup> shows an efficient behavior in the planar case compared to absolute nodal coordinate formulations<sup>(8)</sup>. It is extended to a three-dimensional description using inertial approaches<sup>(9)</sup>, where the physically interpretable EULER-BERNOULLI beam formulation is used. The mathematical derivation is based on the ideas of finite element theory for assembly, and multibody formulations for the evaluation of the equations of motion for each finite element<sup>(10)</sup>.

**3.4.1. Coordinate Settings** Using a general stationary frame of reference, the entire kinematic of one finite element can be described as shown in Fig. 4. Using a reversed Cardan

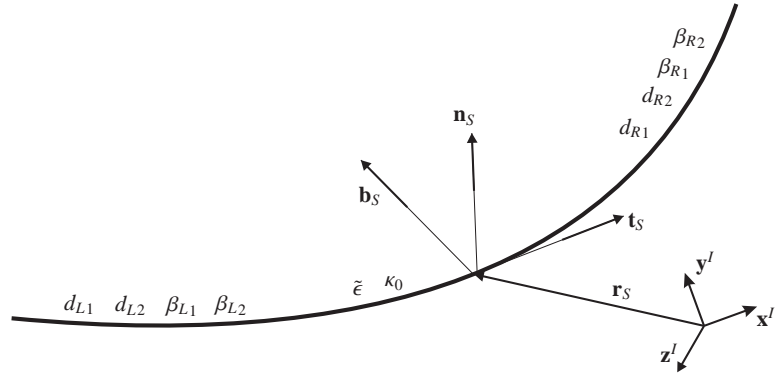


Fig. 4 Internal coordinates.

parameterisation

$$\varphi_0(x) := \varphi_{S_0} + w'_0(x), \quad \varphi_1(x) := \varphi_{S_1} + w'_1(x), \quad \varphi_2(x) := \varphi_{S_2} + w'_2(x) \quad (17)$$

a set of *internal coordinates*

$$\mathbf{q}_i := (x_S, y_S, z_S, \varphi_{S_0}, \varphi_{S_1}, \varphi_{S_2}, \tilde{\epsilon}, d_{L1}, d_{R1}, \beta_{L1}, \beta_{R1}, d_{L2}, d_{R2}, \beta_{L2}, \beta_{R2}, \kappa_0)^T \quad (18)$$

is defined by the position vector and the angle parameterization of the trihedral of the finite element center as well as the longitudinal strain, the coefficients

$$w_i(-l_0/2) := d_{L_i}, \quad w_i(0) := 0, \quad w_i(l_0/2) := d_{R_i}, \quad i = 1, 2, \quad (19)$$

$$w'_i(-l_0/2) := \beta_{L_i}, \quad w'_i(0) := 0, \quad w'_i(l_0/2) := \beta_{R_i}, \quad i = 1, 2 \quad (20)$$

of the ansatz functions with the finite element length  $l_0$  and the torsion

$$\kappa_0 := \mathbf{b} \cdot \mathbf{n}' = w''_0 - \sin(\varphi_{S_1}) w''_2. \quad (21)$$

The degree of the polynomials

$$w_i := a_{w_i} x^5 + b_{w_i} x^4 + c_{w_i} x^3 + d_{w_i} x^2, \quad i = 0, 1, 2 \quad (22)$$

is a compromise between too much stiffening for lower orders and too much support for higher orders with the coefficients of  $w_0$  being constrained by the constant torsion characteristics of (21). In combination, rigid and elastic body motions are decoupled and a compact form of the equations of motion with appropriate approximation not depending on the boundary conditions is available for evaluation.

For coupling of finite elements the global coordinates

$$\mathbf{q}_g := (x_L, y_L, z_L, \varphi_{L_0}, \varphi_{L_1}, \varphi_{L_2}, c_{L_1}, c_{R_1}, c_{L_2}, c_{R_2}, x_R, y_R, z_R, \varphi_{R_0}, \varphi_{R_1}, \varphi_{R_2})^T \quad (23)$$

with

$$c_{L_1} := w_1(-l_0/4), \quad c_{R_1} := w_1(l_0/4), \quad c_{L_2} := w_2(-l_0/4), \quad c_{R_2} := w_2(l_0/4) \quad (24)$$

are used (see Fig. 5) to obtain equations of motion in minimal representation. The information between the coordinate sets is transferred by the motion of the neutral fiber resulting in a transformation  $\mathbf{F}(\mathbf{q}_i, \mathbf{q}_g) = \mathbf{0}$ , which can be solved with NEWTON'S method using analytical JACOBIAN evaluations.

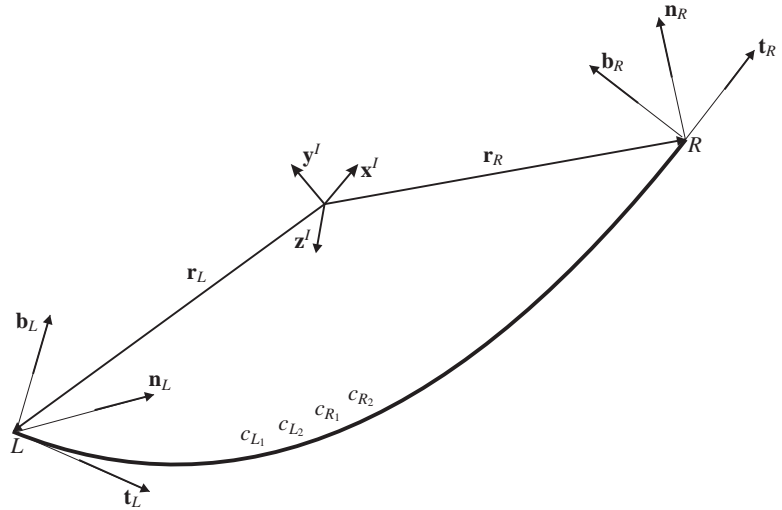


Fig. 5 Global coordinates.

**3.4.2. Equations of Motion** With the LAGRANGIAN formalism

$$\frac{d}{dt} \left( \frac{\partial T}{\partial \dot{\mathbf{q}}_i} \right)^T - \left( \frac{\partial T}{\partial \mathbf{q}_i} \right)^T + \left( \frac{\partial (V_e + V_g)}{\partial \mathbf{q}_i} \right)^T = \mathbf{0} \quad (25)$$

it is possible, to derive the equations of motion with respect to the internal coordinates given the kinetic  $T$ , elastic  $V_e$  and gravitational  $V_g$  energy:

$$\mathbf{M}_i \ddot{\mathbf{q}}_i - \mathbf{h}_i = \mathbf{0} . \quad (26)$$

Globally the equations of motion satisfy

$$\underbrace{\mathbf{J}_{ig}^T \mathbf{M}_i \mathbf{J}_{ig}}_{\mathbf{M}_g} \ddot{\mathbf{q}}_g - \underbrace{\mathbf{J}_{ig}^T (\mathbf{h}_i - \mathbf{M}_i \dot{\mathbf{J}}_{ig} \dot{\mathbf{q}}_g)}_{\mathbf{h}_g} = \mathbf{0} \quad (27)$$

with the JACOBIAN of transformation  $\mathbf{J}_{ig}$ .

**3.4.3. Assembling of the Beam Elements** For coupling the finite elements an extended vector of global coordinates describing the whole beam structure has to be defined. It is given by

$$\mathbf{q}_{ge} := \left( \dots, x_j, y_j, z_j, \varphi_{j,0}, \varphi_{j,1}, \varphi_{j,2}, c_{j,L1}, c_{j,R1}, c_{j,L2}, c_{j,R2}, x_{j+1}, \dots \right)^T . \quad (28)$$

The relationship between the internal coordinates of the  $j$ -th finite element and these extended global coordinates can be written as  $\mathbf{q}_{ij} = \mathbf{Q}(\mathbf{q}_{ge})$ . Then

$$\mathbf{J}_{ijge} := \frac{d\mathbf{q}_{ij}}{d\mathbf{q}_{ge}} \quad (29)$$

is the JACOBIAN matrix of this transformation. For the whole structure with  $k$  finite elements one gets the assembled equations of motion

$$\sum_{j=1}^k \underbrace{\mathbf{J}_{ijge}^T \mathbf{M}_{ij} \mathbf{J}_{ijge}}_{\mathbf{M}_{ge}} \ddot{\mathbf{q}}_{ge} - \sum_{j=1}^k \underbrace{\mathbf{J}_{ijge}^T (\mathbf{h}_{ij} - \mathbf{M}_{ij} \dot{\mathbf{J}}_{ijge} \dot{\mathbf{q}}_{ge})}_{\mathbf{h}_{ge}} = \mathbf{0} . \quad (30)$$

This is a sparse system of equations, which can be implemented very efficiently by index-scanning for used degrees of freedom on the global parts. Then, operations on zero entries can be avoided.

The formulation allows for arbitrary dynamic contact situations as introduced in the previous section, especially non-smooth dynamics including unilateral contacts and dry friction. For the present case, rigid disks are bilaterally bound to the shaft; the two unilateral contacts to the top and bottom circles of the auxiliary bearings are modeled as being rigid with COULOMB friction.

### 3.5. Numerical Framework

Two different groups of numerical schemes can be used to integrate unilateral constrained equations of motion: event-driven and time-stepping schemes<sup>(2)</sup>. The event-driven scheme detects events like detachments or impacts and resolves the exact transition times. Between these events the motion of the system is smooth and all contact laws are reduced to bilateral constraints. Thus the equations of motion can be integrated by a standard ODE/DAE-integrator with root-finding. In contrast, time-stepping methods are based on a time-discretization of the system dynamics including the constraints. A detection of events is not needed and the discretization can be chosen such that the constraints are fulfilled either on position or on velocity level. Moreover, a time-stepping algorithm turns out to be very robust in terms of numerical errors. The described multibody simulation uses a time-stepping method on the velocity level. A detailed description of the numerical framework can be found in<sup>(3)</sup>. A comprehensive review on time integration of non-smooth systems is provided in<sup>(4)</sup>.

### 3.6. Co-simulation with Simulink

A co-simulation between MBSim and MATLAB/SIMULINK is used to integrate the feedback controller. MATLAB provides an Application Programming Interface (API) called "MATLAB engine", which allows calls to MATLAB from C as a computation engine. The MATLAB engine communicates with a separate MATLAB process via pipes (in Unix) and through ActiveX on Microsoft Windows. There is a library of functions that allows start and end of a process, sending of data to and from MATLAB, and sending of commands to be processed.

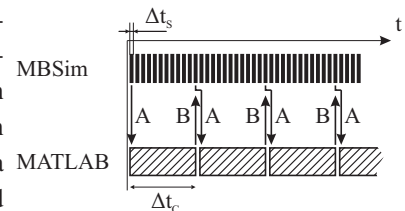


Fig. 6 Co-simulation

Figure 6 shows the synchronization of the co-simulation. The feedback controller is calculated in MATLAB/SIMULINK with a fixed time step size of  $\Delta t_c$  using an EULER discretization as it is used at the experimental test rig. The simulation is calculated with the much lower fixed time step size  $\Delta t_s$  of the time stepping integrator. The synchronization starts with "A". The positions and velocities, which are used by the feedback controller, are transferred to MATLAB and one calculation step of the controller is started in MATLAB. In the meantime the multibody simulation MBSim executes until the end of the controller time step  $\Delta t_c$  is reached. With the synchronization "B" the calculated control force for the actuators is transferred to MBSim and the actuator force in the multibody simulation is updated.

The advantages of the co-simulation are as follows. Since the dSPACE real-time hardware uses SIMULINK for the code generation of the controller, a single SIMULINK model of the controller can be used for both - simulation and experiment. So a very rapid controller development and optimization can be achieved. There is also no error source caused by the modeling of the test rig controller in another simulation software. Also, the co-simulation takes advantage of recent multi-core processors, because between the synchronization steps MBSim and MATLAB are two independent processes.

## 4. Test rig

To verify the developed concept, a test rig, which has been developed at the University of Bath<sup>(21)</sup>, is used.

The rotor/magnetic bearing system consists of two active magnetic bearings and two active auxiliary bearings (Fig. 7). The rotor is 600 mm long and 30 mm in diameter with two magnetic bearing cores and two collars. Each collar is positioned along the rotor at an auxiliary bearing. The collar diameter and surface finish/materials determines the rotor/auxiliary bearing clearance gap and contact friction. The complete rotor mass is 6.5 kg. The active magnetic bearings are eight-pole types configured to operate as opposing pairs and positioned at

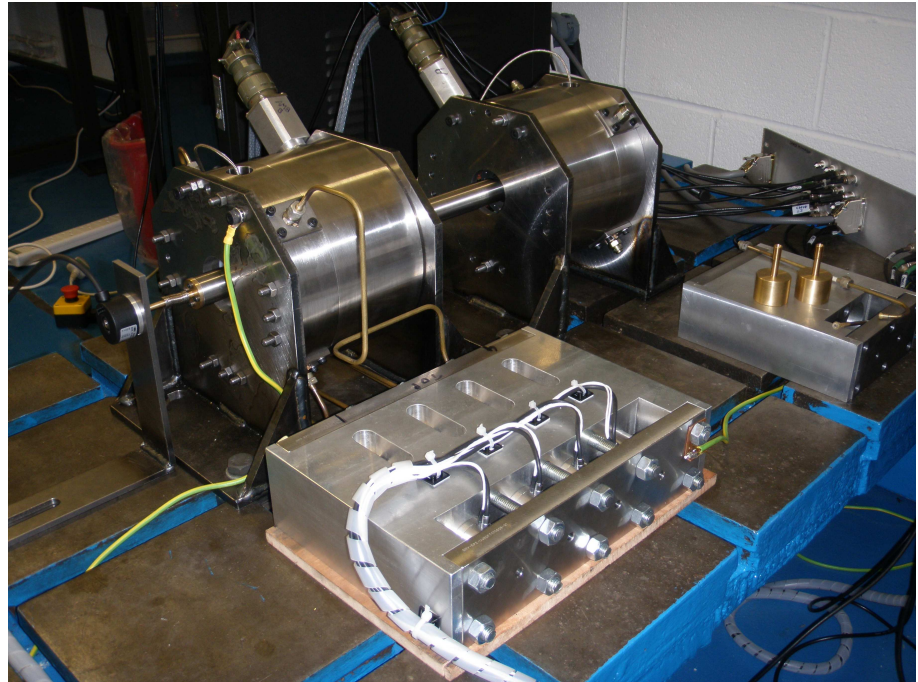


Fig. 7 Test Rig

45deg to the vertical to maximize static load capacity. The magnetic bearing core/stator clearance gap is 0.8 mm and the maximum force capacity of the bearings is 2.6 kN. Performance roll-off occurs at 275 Hz. The magnetic bearings have a negative stiffness of 3.9 MN/m. Rotor position is measured using eddy current sensors located adjacent to each magnetic bearing. The active auxiliary bearings are also located adjacent to the position sensors. Initial control of the rotor is achieved using local proportional-integral-differential (PID) feedback. Controller gains  $k_p = 5.1$  MN/m,  $k_i = 0.01$  MNsm and  $k_d = 0.05$  MNs/m provide a stable rotor with low damping characteristics. The PID controlled rotor has natural frequencies at 1049 rad/s (mainly rigid body mode), 1252 rad/s (mainly rigid body mode), 2329 rad/s (first bending mode) and 4599 rad/s (second bending mode).

### 5. Modeling

The simulation model of the rotor system shown in Fig. 8 comprises a 3D flexible rotor, 4 rigid disks, 2 auxiliary bearings, the disk of the motor, the flexible shaft coupling and two unilateral rigid contacts between the auxiliary bearing disks and the auxiliary bearings. Additionally, unbalance masses can be added to every disk. The shaft coupling is modeled as a spatial spring-damper-element. The disk of the motor is coupled to the environment using spring-damper-elements. The mathematical modeling of the components is described in Section 3.

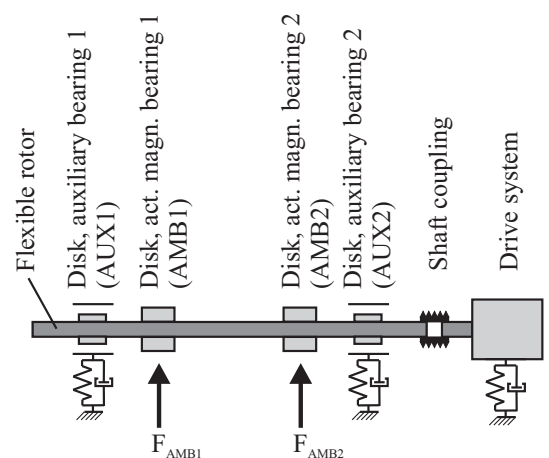


Fig. 8 Modeling

#### 5.1. Modeling of the auxiliary bearing

The auxiliary bearings are ball bearing types, which are modeled using a ring having

one rotational degree of freedom. This degree of freedom is damped, which represents the friction of the bearing. The unilateral contact with the inner surface of this ring is modeled as a spatially rigid contact with friction.

## 5.2. Modeling of faults

As mentioned in section 2, the modeling of four faults is provided. The following embedded faults have been selected:

- Unbalance masses
- Angular misalignment between the rotor shaft and the motor
- Cut-off of one or more channels of the AMBs
- Disturbance of one or more channels of the AMBs

## 6. Experimental study: Rotor drop at 2700 rpm

Various experiments of rubbing with and without controlled auxiliary bearings have been performed. A rotor drop has been chosen as an example to show the possibilities of the concept of condition monitoring. For this experiment, the rotor is running at a constant speed of 2700 rpm and at a time of  $t=0.5$ s both AMBs are switched off. Both auxiliary bearings are used as passive / conventional backup bearings. The example starts with Phase B, where the measurement is treated. It is assumed that the monitoring system detected the fault and already captured the sensor signals (Phase A).

**Phase B: Identification of failure** The identification procedure uses the measurement of the rotor drop: the rotor orbit next to the auxiliary bearing 1 (Fig. 9, left); and next to the auxiliary bearing; and the control currents of the AMB channels (Fig. 10). For comparison of measurement and simulation the rotor speed is shown additionally, see Fig. 9, right.

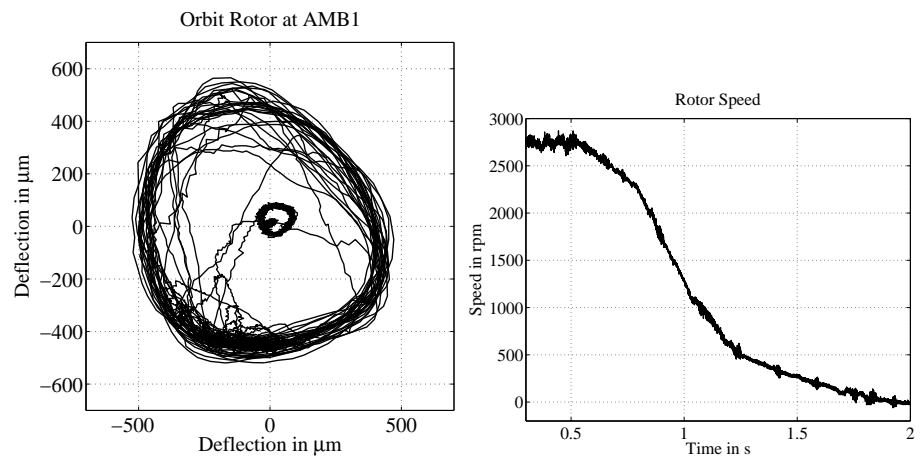


Fig. 9 Experiment: rotor orbit at auxiliary bearing 1 (left), rotor speed (right)

As shown in figure 2, the procedure of the identification runs through various checks. In the presented example, the first check already determines the fault, which is a *“Cut-off of all channels of the AMBs”*. The fault parameter, which is used in the simulation, is a factor of all control current channels: *“Factor of control currents = 0”*.

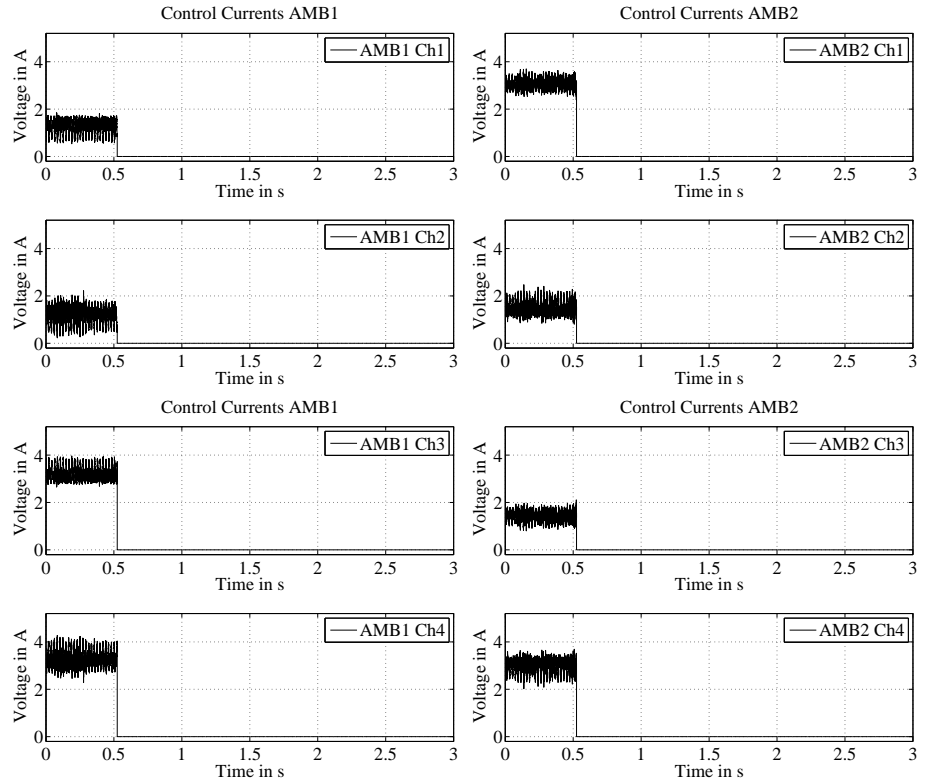


Fig. 10 Measurement of the control currents of the AMBs

**Phase C: Simulation, Optimization**

Using the determined fault, the simulation is configured. All fault parameters from detected faults, are set to the initial, no-fault values. The only unknown parameter is the friction coefficient of the contacts, which is assumed to be transient over the life-time of a auxiliary bearing. In this example it is assumed that both auxiliary bearings have the same friction coefficient.

As discussed in section 2, the slope of the polar angle of the contact point of the auxiliary bearing 1 has been evaluated (Fig. 11). In the presented example it has been found that in all experiments, the same rubbing state has been established in both auxiliary bearings. For that reason, only auxiliary bearing 1 was evaluated. The slope shows clearly the occurrence of the rubbing state.

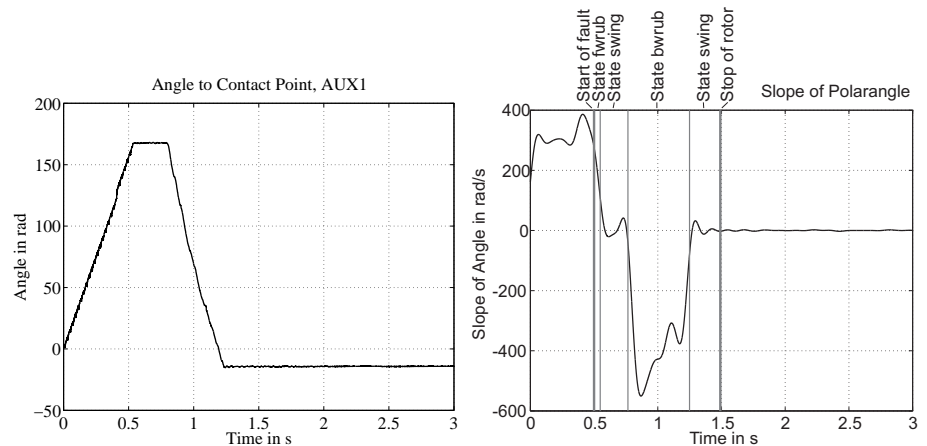


Fig. 11 Determination of the polar angle to the contact point at AUX1 (left) and its slope (right)

The duration of the occurrence of the certain rubbing states is evaluated from the slope, and is used for calculating the cost function.

One run of the simulation is established from an initial phase of rotation at the measured rotational speed, where the initial transient effects decay, followed by the incidence of the fault. The evaluation of the cost function takes the time from the occurrence of the fault until the rotor is stopped.

Using the optimization algorithm *implicit filtering* the unknown friction coefficient has been successfully determined after several iterations. Using the determined parameter, the alignment of simulation and measurement is very good. The simulated rotor orbits at the auxiliary bearing 1 is shown in Fig. 12, left. The rotor speed of the simulation is shown in Fig. 12, right. The simulated speed matches the measured speed very well.

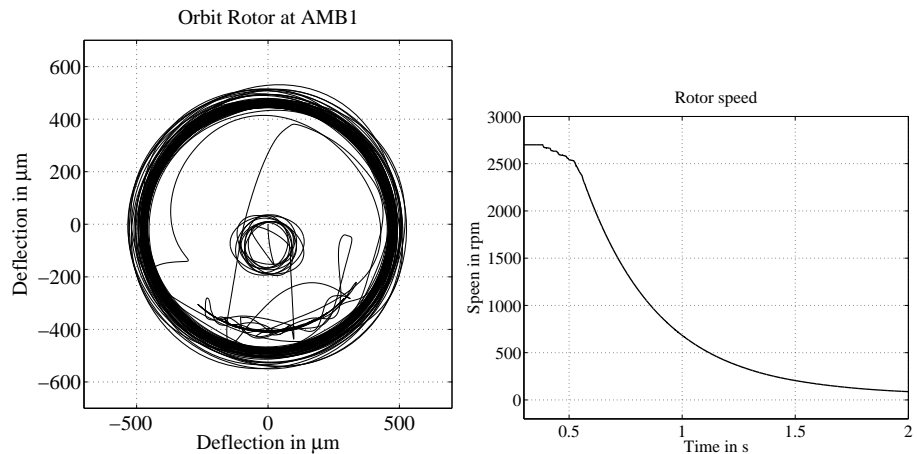


Fig. 12 Simulation: rotor orbit at auxiliary bearing 1 (left), rotor speed (right)

**Phase D: Storage of contact event** As described in the concept, the simulation data of the contact event are stored.

**Phase E: Evaluation of auxiliary bearing condition** Depending on the application and the type of auxiliary bearing, several kinds of evaluation of the contact event are conceivable.

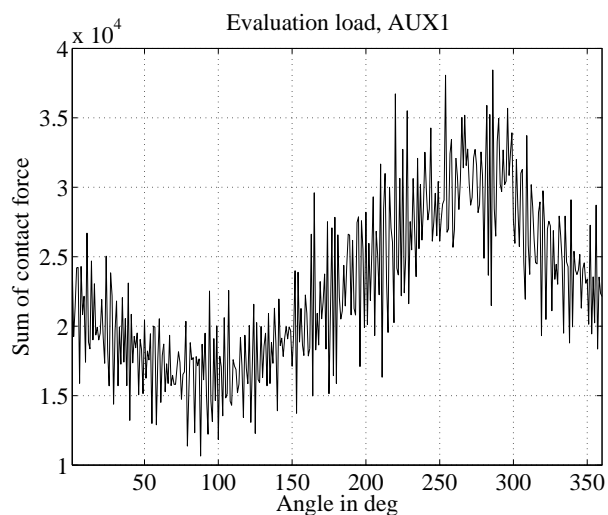


Fig. 13 Evaluation of two contact events

In the presented example, the sum of the contact forces vs. the polar angle in auxiliary bearing 1 is evaluated. As a result, the distribution of the resulting contact forces - superposition of normal and tangential forces - over the surface of the auxiliary bearing is performed, which gives information of the wear of the surface. The evaluation of the two contact events

is shown in Fig. 13. One can see, that depending on the various contact events, a distinctive distribution of the load over the surface is calculated. The area with the maximum load limits the life-time of the auxiliary bearing.

## 7. Conclusions

A new concept for model-based condition monitoring of auxiliary bearings has been developed. After each contact event, the measured data are evaluated in several steps. Using this evaluation the number of modeled faults is reduced to the fault, which leads to rubbing. An optimization algorithm aligns a sophisticated simulation of the rotor system, including the fault, with the measurement. The simulation data of the contact event are stored. Following each contact event, the stored data of all occurred contacts are evaluated, giving an estimation about the life expectancy of the auxiliary bearing. A test rig has been used to proof the concept. The test rig consists of a rotor shaft, two magnetic bearings and two auxiliary bearings. An experiment involving cut-off of the AMBs followed by a rotor drop is evaluated by the concept. The fault is identified. After the optimization, the simulation aligns very well with the measurement. The determined simulation data of the contact event allow an accurate estimation of the condition of the auxiliary bearings.

## Acknowledgment

This work was supported by a fellowship within the Postdoc-Programme of the German Academic Exchange Service (DAAD).

## References

- (1) B. Brogliato, A. A. Ten Dam, L. Paoli, F. Gnot, and M. Abadie. Numerical simulation of finite dimensional multibody nonsmooth mechanical systems. In *ASME Applied Mechanics Reviews*, 2002.
- (2) M. Förg. *Mehrkörpersysteme mit mengenwertigen Kraftgesetzen - Theorie und Numerik*. Number Nr. 20 in Fortschrittberichte VDI. VDI-Verlag, Düsseldorf, 2007.
- (3) M. Förg, R. Zander, and H. Ulbrich. A framework for the efficient simulation of spatial contact problems. In *Proc. of the ECCOMAS Conference on Multi-Body Systems*, Milano, Italy, 2007.
- (4) Ch. Studer. Augmented time-stepping integration of non-smooth dynamical systems. In *ETH E-Collection*, 2008.
- (5) R. Zander, Th. Schindler, M. Friedrich, R. Huber, M. Förg, and H. Ulbrich. Non-smooth dynamics in academia and industry: recent work at TU München. In *Acta Mechanica*, 2008.
- (6) T. Wasfy and A. Noor. Computational strategies for flexible multibody systems. In *Appl Mech Rev*, 2003, vol. 56, pages 553-613, ASME, New York.
- (7) R. Zander. Flexible multi-body systems with set-valued force laws. In *Fortschritt-Berichte VDI : Reihe 20, Rechnerunterstützte Verfahren*, 2009, Vol. 420, Düsseldorf.
- (8) A. Shabana, O. Bauchau and G. Hulbert. Integration of Large Deformation Finite Element and Multibody System Algorithms. In *J Comput Nonlinear Dynamik*, 2007, Vol. 2, pages 351-359, ASME, New York.
- (9) J. C. Simo and L. Vu-Quoc. A geometrically-exact rod model incorporating shear and torsion-warping deformation. In *Int J Solid Struct*, 1991, Vol. 27, Elsevier, New York.
- (10) T. Schindler, M. Friedrich and H. Ulbrich. Computing Time Reduction Possibilities in Multibody Dynamics. In *Multibody Dynamics: Computational Methods and Applications; Computational Methods in Applied Sciences*, Springer, Dordrecht, to appear 2010.
- (11) M. N. Sahinkaya, M. O. T. Cole and C. R. Burrows. Fault detection and tolerance in synchronous vibration control of rotor-magnetic bearing systems. In *Proc. Instn. Mech. Engrs., Part C, Journal of Mechanical Engineering Science*, 215 (C12), 2001.
- (12) B. Heckmann, L. Ginzinger, H. Ulbrich. Model-based Identification of Unbalance and

- Angular Misalignment in a Rotor System. In *Proc. of the Thirteenth International Symposium on Transport Phenomena and Dynamics of Rotating Machinery (ISROMAC-13)*, April 4-9, 2010, Honolulu, USA, to appear.
- (13) C. T. Kelley. Iterative Methods for Optimization. In *Frontiers in Applied Mathematics*, SIAM, 1999 .
  - (14) U. Ehehalt, R. Markert. Rotor motion during stator contact. In *Proc. of the 6th IFToMM Conf. on Rotor Dynamics*, Vol. 2, Editors E. J. Hahn and R. B. Randall, Sydney, 2002.
  - (15) C. R. Burrows, P. S. Keogh, M. N. Sahinkaya . Progress towards smart rotating machinery through the use of active bearings. In *Proc. IMechE, Part C: Journal of Mechanical Engineering Science*, Volume 223, Number 12 / 2009.
  - (16) P. M. Frank, X. Ding. Frequency domain approach to optimally robust residual generation and evaluation for model-based fault diagnosis. In *Automatica(Oxford)*, Volume 30, Number 5, Elsevier, 1994.
  - (17) M. O. T. Cole, P. S. Keogh, M. N. Sahinkaya, C. R. Burrows. Towards fault-tolerant active control of rotor-magnetic bearing systems. In *Control Engineering Practice*, Volume 12, Number 4, Elsevier, 2004.
  - (18) I. S. Cade, P. S. Keogh, M. N. Sahinkaya. Fault identification in rotor/magnetic bearing systems using discrete time wavelet coefficients. In *IEEE ASME TRANSACTIONS ON MECHATRONICS*, Volume 10, Number 6, 2005.
  - (19) A. H. G. Abulrub, M. N. Sahinkaya, C. R. Burrows, P. S. Keogh. Performance assessment of a multi-frequency controller applied to a flexible rotor magnetic bearing system-contact dynamics. In *Motion and Vibration Control: Selected Papers from Movic 2008*, Springer, 2008.
  - (20) A. H. G. Abulrub, M. N. Sahinkaya, P. S. Keogh, C. R. Burrows. Adaptive Control of Active Magnetic Bearings to Prevent Rotor-Bearing Contact. In *Proc. of ASME International Mechanical Engineering Congress and Exposition (IMECE2006)*, November 5-10, 2006, Chicago, Illinois, USA.
  - (21) I. S. Cade, M. N. Sahinkaya, C. R. Burrows, P. S. Keogh. An active auxiliary bearing control strategy to reduce the onset of asynchronous periodic contact modes in rotor/magnetic bearing systems. In *Proceedings of ASME Turbo Expo 2009: Power for Land, Sea and Air (GT2009)*, June 8-12, 2009, Orlando, Florida, USA.